Title

Inductance Investigation of $YBa_2Cu_3O_{7-\delta}$ Nano-Slit SQUIDs Fabricated With a Focused Helium Ion Beam

Journal

IEEE Transactions on Applied Superconductivity, 29(5)

ISSN

1051-8223

Authors

Li, Hao
Cho, Ethan Y
Cai, Han
et al.

Publication Date

2019

DOI

10.1109/tasc.2019.2898692

Peer reviewed

Inductance Investigation of $YBa_2Cu_3O_{7-\delta}$ Nano-Slit SQUIDs Fabricated With a Focused Helium Ion Beam

Hao Li, Ethan Y. Cho, Han Cai, Yan-Ting Wang, Stephen J. McCoy, and Shane A. Cybart

(Invited Paper)

***Abstract*—Focused helium ion beam material modification is ideally suited for the fabrication of $YBa_2Cu_3O_{7-\delta}$ (YBCO) Josephson junctions and superconducting feature sizes down to the nanoscale. We report the fabrication and measurement of YBCO nano-slit SQUIDs and study how scaling the dimensions of the SQUID body and electrodes influences the electrical properties. Sixteen nano-slit SQUIDs with different width and length were fabricated from a single-layer 25-nm-thick YBCO film. The experimental results yield an estimation of the sheet inductance to be ∼4 pH/□ and a penetration depth of ∼180 nm. The temperature dependence of the inductance agree well with an impurity scattering model, indicating that the T_C of the film was ∼82 K, and the ratio between geometric inductance and kinetic inductance at 0 K was ∼0.8. These results provide solid basis for the design of high-performance, high-T_C micro-SQUID magnetometers.**

***Index Terms*—Nano-slit SQUID, focused helium ion beam, inductance, YBCO thin film.**

I. Introduction

FOCUSED helium ion beam (FHIB) materials modification is an emerging technique with the capability to make high-quality thin-film, high-transition temperature (high-T_C) superconducting Josephson junctions [1]. In this method, ion irradiation converts the film from a superconductor to an insulator by disordering the crystalline lattice [2]. In contrast to other techniques to fabricate high-T_C superconducting devices based on grain-boundary [3], step-edge [4], or multilayer c-axis sandwich Josephson junctions [5], no material is removed or etched, as a result, nanoscale insulating features are obtainable for both Josephson junctions [6] and superconducting electrodes for devices such as superconducting quantum interference devices (SQUIDs) [7]. Scaling down to smaller junction and SQUID loop dimensions are necessary for higher integration density of superconducting circuits and for improving performance [8]. The smaller dimensions obtainable in circuit geometry afforded by scaling yields more control over circuit parameters such as critical current I_C, resistance R and inductance L, the key variables for optimization of SQUIDs.

Recently, we developed a low-noise micro magnetometer based on a nano-slit SQUID using the FHIB materials modification technique to create both the junctions and the SQUID loop without any hard mask or milling process. A magnetometer was demonstrated that featured a 10 nm × 20 μm slit that allowed for a large inductive coupling between a 100×100 μm^2 area flux concentrating pick-up loop to the SQUID [9]. The nano-slit was instrumental in obtaining a high magnetic field sensitivity of 4 pT/Hz$^{1/2}$ for such a small area sensor. This motivates a more thorough investigation into the optimization of the nano-slit geometry. Here, we further investigate nano-slit SQUID devices with a detailed investigation into the geometric variables for insight into the maximization of inductive coupling to flux concentrators. Specifically we compare the electrical transport properties of nano-slit SQUIDs with different slit dimensions (width and length) and how device performance is affected by changes in temperature.

II. Experiment

For this experiment, commercial 25 nm thick YBCO thin-films were grown on cerium oxide buffered r-plane sapphire by reactive coevaporation. A subsequent 200 nm thick layer of gold was thermally evaporated *in-situ* for electrical contacts. Wafers were diced into 5 mm × 5 mm chips. Substrates and large-scale electrodes were patterned into both the gold and YBCO layers using photolithography and argon ion milling. A second photolithography step and chemical etch were used to remove the gold from the area intended for FHIB direct writing, as shown in Fig. 1(a). Our test circuit layout was designed to

Manuscript received October 30, 2018; accepted January 8, 2019. Date of publication February 11, 2019; date of current version March 15, 2019. This work was supported in part by the Air Force Office of Scientific Research under Grant FA955015-1-0218, in part by the National Science Foundation under Grant 1664446, in part by the National Institutes of Health under Contract No. j1R43EB023147-01, in part by the University of California Office of the President, Multicampus Research Programs and Initiatives under Award No. 009556-002, and in part by the Army Research Office Grant W911NF1710504. *(Corresponding author: Shane A. Cybart.)*

H. Li, E. Y. Cho, and H. Cai are with the Department of Mechanical Engineering, University of California, Riverside, CA 92521 USA (e-mail: haoli@ucr.edu; eycho@ucr.edu; hcai017@ucr.edu).

Y.-T. Wang and S. J. McCoy are with the Department of Materials Science and Engineering, University of California, Riverside, CA 92521 USA (e-mail: ywang502@ucr.edu; smcco003@ucr.edu).

S. A. Cybart is with the Department of Mechanical Engineering and the Department of Materials Science and Engineering, University of California, Riverside, CA 92521 USA (e-mail: cybart@ucr.edu).

Color versions of one or more of the figures in this paper are available online at http://ieeexplore.ieee.org.

Digital Object Identifier 10.1109/TASC.2019.2898692

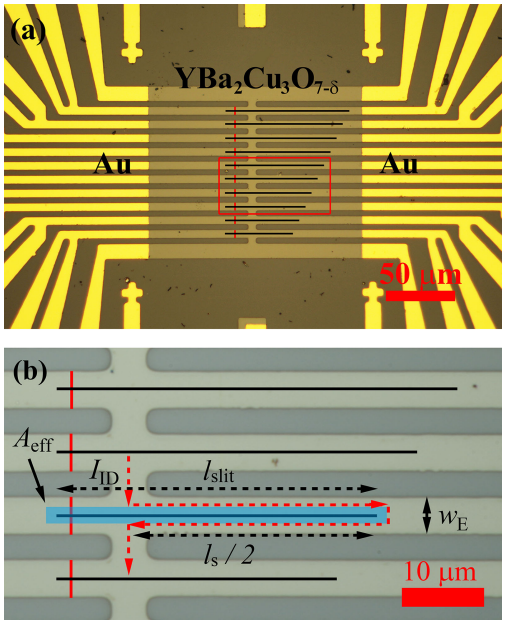

Fig. 1. (a) YBCO Nano-slit SQUIDs optical photograph. (b) Zoomed in view, the red solid lines represent the light helium ion irradiation for junction writing, and the black lines represent the helium ion irradiation for nano-slit writing.

support several YBCO 4 μm (or 8 μm, 16 μm) wide strip lines within a small 100 $\times$ 100 μm^2 area in the center of the substrate. The close spacing of the devices was engineered to reduce errors associated with material and process non-uniformities.

Following photographic patterning, samples were loaded into an Orion Plus Helium Ion Microscope for FHIB direct write patterning using a 0.5 nm diameter, 32 keV helium ion beam. Fig. 1(b) shows an optical photograph of a sample with several YBCO strip lines, along with the FHIB irradiation patterns used to create nano-slit SQUIDs. The Josephson junctions (vertical lines) and nano-slit SQUID loop (horizontal lines) were irradiated using dosages of 8 $\times$ 10^{16} He +/ cm^2 and 8 $\times$ 10^{17} He + /cm^2 respectively.

In contrast to conventional low-T_C or high-T_C SQUIDs, the nano-slit SQUIDs have no physical hole in the material but rather an insulating region contained within a contiguous film. This innovation allows for the patterning of sub-10nm features in contrast to conventional argon ion beam etching, which degrades the superconductivity of YBCO when the feature sizes approach dimensions less than $\sim$1 μm [10].

We fabricated 16 nano-slit SQUID test devices in total. The width of the electrodes w_E ranges from 4 μm to 16 μm, while the length of the slit l_{slit} from 10 μm to 70 μm. The nano-slit SQUIDs were cooled in an evacuated dip probe with a cryoperm shield in liquid helium. Typical current-voltage characteristics (*I-V*) are shown in Fig. 2(a) for four temperatures 9 K, 24 K, 33 K, and 58 K. The paralleled Josephson junctions exhibited critical currents and resistances that ranged from 450 μA, 265 μA, 155 μA to 20 μA and 3.5 Ω, 3.3 Ω, 2.9 Ω to 2.5 Ω respectively. The resistance of these devices slightly decreased with increasing temperature for such a wide temperature range ($\sim$50 K) suggesting that the Josephson effect comes

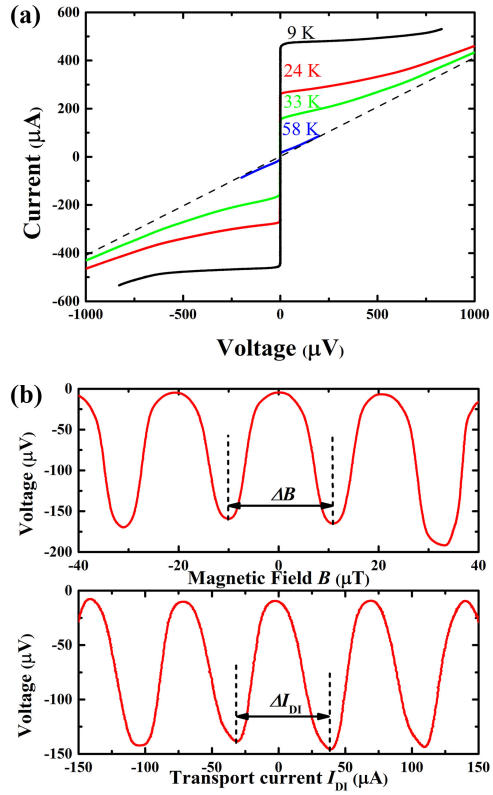

Fig. 2. (a) The *I-V* curves of the nano-slit SQUID with 4 μm width and 40 μm length at 9, 24, 33, and 58K; (b) The voltage modulation of field (*V-B*) and transport current (*V-*I_{DI}) of the nano-slit SQUID measured at about 9 K.

from tunneling through an insulating barrier rather than Andrew reflection of a normal metal [6].

The SQUIDs were then statically biased just above I_C and voltage was measured as magnetic field was swept using an external coil. Typical voltages ranged from 10 μV to 250 μV. We remark that very large voltages are possible due to the high junction resistances obtainable with FHIB. To investigate the inductance of the YBCO thin film strip line, direct inject transport current I_{DI} was directly introduced into the superconducting loop of the nano-slit SQUID as illustrated in Fig. 1(b). The voltage modulation of field (*V-B*) and transport current (*V-*I_{DI}) were recorded in Fig. 2(b) at about 9 K.

III. Results and Discussion

When a uniform perpendicular magnetic field *B* is applied to the nano-slit SQUIDs, the magnetic flux threading the slit per unit length Φ /l_{slit} is [11]

$$\frac{\Phi}{l_{slit}} = w_E B + \frac{\mu_0}{2\pi}\int_{-w_E/2}^{w_E/2} J(x)\ln\left|\frac{w_E/2 - x}{w_E/2 - x}\right| dx, \qquad (1)$$

where w_E is the width of the electrode as illustrated in Fig. 1(b), and $J(x)$ is the supercurrent distribution along the wide direction. Although the expression of $J(x)$ is usually non-analytical or complicated, a uniform current distribution $J(x)$ is a reasonable start point of discussion in the thin film limit ($t << \lambda$, where t is the thickness of the film and λ is the London penetration

depth), especially when the w_E is comparable to λ_{eff} $\sim\lambda^2/t$, similar to the current distribution in the center line of a coplanar waveguide [12]. According to the model of a thin film strip line in a perpendicular field, $J(x)$ with a uniform distribution is supposed as

$$J(x) = \begin{cases} -\frac{2B}{\mu_0}, -w_E/2 < x < 0 \\ \frac{2B}{\mu_0}, 0 < x < w_E/2 \end{cases}, \quad (2)$$

then we can get the integration from Eq. (1) to be

$$\Phi = w_E l_{slit} B\left(1 - \frac{2\ln 2}{\pi}\right) \approx 0.56 w_E l_{slit} B. \quad (3)$$

In the limit where, $w_E >> \lambda_{eff}$, the numerical results show $\Phi \sim 0.44 w_E l_{slit} B$. We can also model it by drawing insight from similar approaches used to study flux focusing in planar junctions [13]. When a magnetic field line impinges on a superconducting thin film, it will be redirected to the nearest edges of the film in order to minimize the electromagnetic free energy. The flux in the area where the point is closer to the junction slit than other edges contributes to the total threading magnetic flux to the junction. In this manner, the total magnetic flux Φ is represented as B multiplied by an effective area A_{eff}, which was theoretically and experimentally shown to be proportional to $w^2/2$, where w is the width of the planar junction. In this similar case, the effective area for the nano-slit SQUID from the geometry should be proportional to $\sim w_E l_{slit}/2$, as shown in Fig. 1(b).

In Fig. 3(a), we show the magnetic field periodicity ΔB determined from the *V-B* measurements [see Fig. 2(b)] plotted as a function of the slit length. Effective area $A_{eff} = \Phi_0/\Delta B$ was calculated and shown with a linear fit to the data. We observed that the A_{eff} of the nano-slit SQUIDs was proportional to l_{slit} and w_E with slope coefficients close to the value in Eq. (3). Furthermore, the nonzero y-intercept in Fig. 3(a) may be attributed to two things, first, the actual slit length which the magnetic field can go through is $l_{slit}+2\lambda_{eff}$, where λ_{eff} is $\sim$1.3 μm when λ $\sim$180 nm and t $\sim$25 nm; second, the measurement errors of the effective areas in the experiments, as shown in Fig. 3(a), the number of devices with larger length is not as many as the devices with lower length.

To investigate inductance properties, we equate the applied magnetic field periodicity with that obtained from the direct inject transport current I_{DI} [see Fig. 2(b)] for several devices. When a current I_{DI} is directly injected into the nano-slit SQUID loop, the magnetic flux coupled to the SQUID equals the product of I_{DI} and the inductance L_s of the path of strip line. The inductance L_s, is therefore the flux quantum Φ_0 divided by ΔI_{DI}. In a superconducting thin film, the inductance L_s consists of geometric inductance L_g and the temperature dependent kinetic inductance L_k. Again, assuming a uniform supercurrent distribution in the thin film, L_k is $\sim 2\mu_0\lambda^2 l_s/w_E t$, where l_s is the total length of strip line. According to a model for d-wave superconductors with impurity scattering [14], [15], the λ(T) has

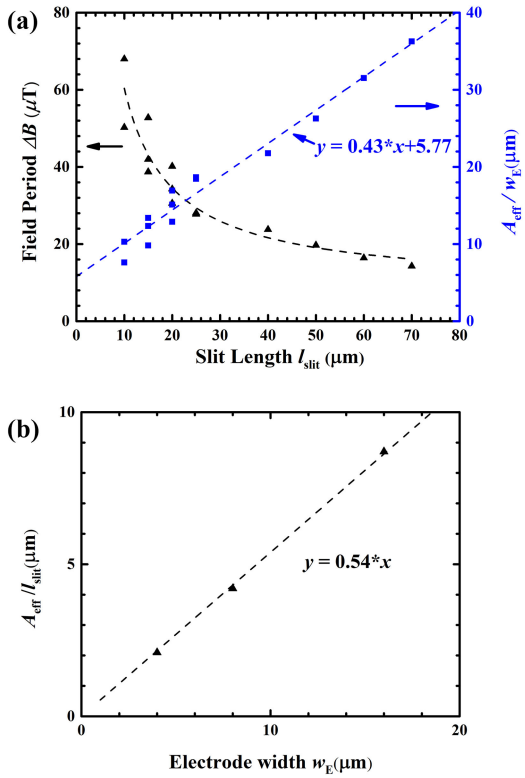

Fig. 3. (a) The effective area per unit width A_{eff} / w_E scaled with the slit length with fixed width 4 μm. (b) the effective area per unit length A_{eff} /l_{slit} scaled with the width of the nano-slit SQUID. The data were taken at about 9 K.

a temperature dependence of the form

$$\lambda(T) = \frac{\lambda(0)}{\sqrt{1-(T/T_C)^2}}, \quad (4)$$

which yields

$$L_s = L_g + L_k(0)/[1-(T/T)^2]. \quad (5)$$

The inductance of the strip line shared by the transport current path and the SQUID loop was extracted according to $L_s = \Phi_0/\Delta I_{DI}$. The dependence between L_s and the strip line dimension yeild 4 pH/□, as shown in Fig. 4(a). We built a model with the same design of those devices in the simulation tool InductEx [16], the London penetration depth is the only variable in this model, as shown in Fig. 4(b), and the value matching the experiment data the best is 180 nm, which would be used for circuit design in the future.

To further investigate the temperature dependence of the inductance, we compare measurements taken at different temperature. The direct inject current period ΔI_{DI} decreased as the temperature increased implying an increase in inductance L_s, as shown in Fig. 5. The results fit well with the theoretical model of the Eq. (5), and indicate that the $L_g/L_k(0)$ was $\sim$0.8. By using $L_k(0) \sim 2\mu_0\lambda(0)^2 l_s/w_E t$, we could deduce that the $\lambda(0)$ was $\sim$210 nm, which in turn shows that the extracted $L_k(0)$ is in a reasonable range.

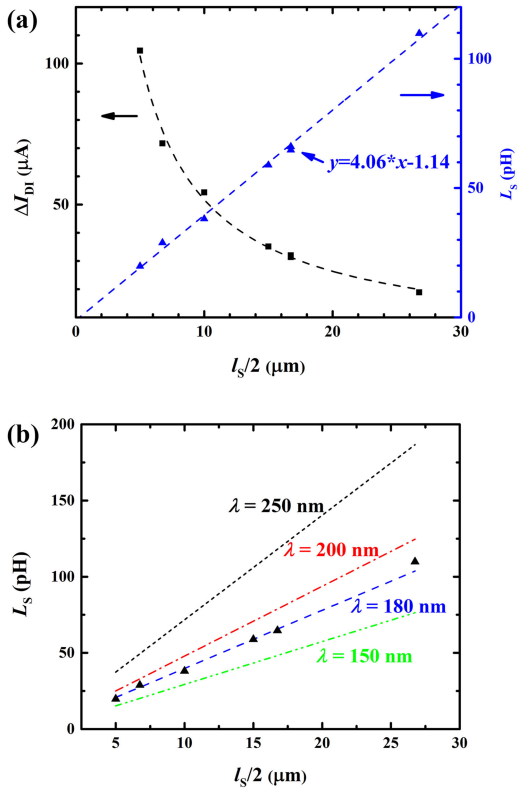

Fig. 4. (a) The inductance L_s scaled with the length of the YBCO thin film strip line with 2 μm width, gave an estimation of 4 pH/□. (b) Simulation model compared with experiment suggesting a $\lambda \sim$180 nm.

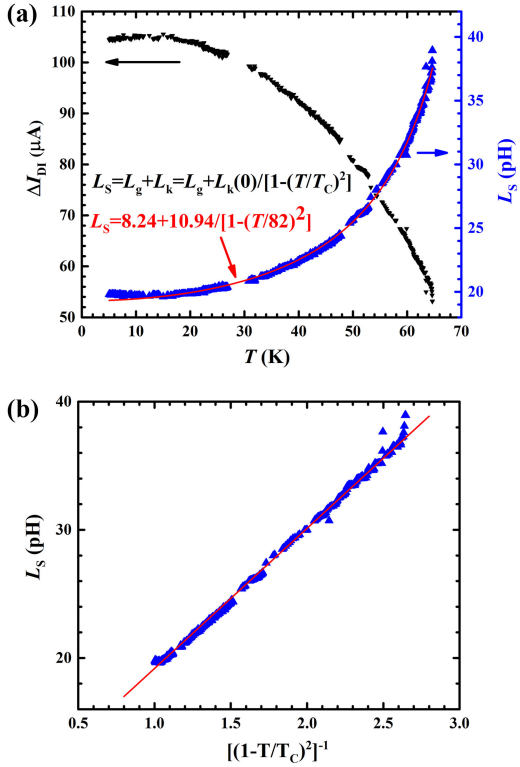

Fig. 5. (a) The temperature dependence of the inductance of superconducting thin film stripe-line 4 μm wide and 5 μm long, which suggested the $T_c \sim$82 K, $L_g/L_k(0) \sim$0.8, and $\lambda(0) \sim$210 nm.

IV. Conclusion

Nano-slit SQUIDs with different width and length were designed and fabricated by FHIB. The response to an external uniform magnetic field of these SQUIDs was explained by flux focusing effect. The inductance of the YBCO thin film strip line was thoroughly investigated. The inductance per square of our 25 nm thick YBCO thin films were estimated to be $\sim$4 pH/□, with a $\lambda(0) \sim$180 nm. The temperature dependence of the inductance of YBCO thin film was explained by a theoretical model for a d-wave superconductor, and the fittings gave an estimation of $L_g/L_k(0) \sim$0.8. These results provide a wealth of knowledge into the optimization and the design of future devices. The much improved sensitivity over similarly sized prior-art devices [17] suggest a new nano-slit approach to compact multi SQUID arrays [18].

References

[1] S. A. Cybart *et al.*, "Nano Josephson superconducting tunnel junctions in $YBa_2Cu_3O_{7-\delta}$ directly patterned with a focused helium ion beam," *Nature Nanotechnol.*, vol. 10, pp. 598–602, Jul. 2015.

[2] A. E. White *et al.*, "Ion-beam-induced destruction of superconducting phase coherence in $YBa_2Cu_3O_{7-\delta}$," *Phys. Rev. B, Condens. Matter*, vol. 1, pp. 3755–3758, Mar. 1988.

[3] D. Gustafsson, H. Pettersson, B. Iandolo, E. Olsson, T. Bauch, and F. Lombardi, "Soft nanostructuring of YBCO Josephson junctions by phase separation," *Nano Lett.*, vol. 10, pp. 4824–4829, Nov. 2010.

[4] M. I. Faley *et al.*, "High-Tc DC SQUIDS for magnetoencephalography," *IEEE Trans. Appl. Supercond.*, vol. 23, no. 3, Jun. 2013, Art no. 1600705.

[5] K. Hirata *et al.*, "Tunneling measurements on superconductor/insulator/superconductor junctions using single crystal $YBa_2Cu_3O_{7-\delta}$ thin films," *Appl. Phys. Lett.*, vol. 56, Feb. 1990, Art. no. 683.

[6] E. Y. Cho *et al.*, "$YBa_2Cu_3O_{7-\delta}$ superconducting quantum interference devices with metallic to insulating barriers written with a focused helium ion beam," *Appl. Phys. Lett.*, vol. 106, Jun. 2015, Art. no. 252601.

[7] E. Y. Cho, Y. W. Zhou, J. Y. Cho, and S. A. Cybart, "Superconducting nano Josephson junctions patterned with a focused helium ion beam," *Appl. Phys. Lett.*, vol. 113, Jul. 2018. Art. no. 022604.

[8] J. Clarke, and A. I. Braginski, eds., *The SQUID Handbook: Applications of SQUIDs and SQUID Systems*. New York, NY, USA: Wiley, 2006.

[9] E. Y. Cho, H. Li, J. Lefebvre, Y. W. Zhou, R. C. Dynes, and S. A. Cybart, "Direct-coupled micro-magnetometer with Y–Ba–Cu–O nano-slit SQUID fabricated with a focused helim ion beam," *Appl. Phys. Lett.*, vol. 113, Oct 2018, Art. no. 6591.

[10] F. Herbstritt, T. Kemen, A. Marx, and R. Gross, "Ultraviolet light assisted oxygenation process for submicron $YBa_2Cu_3O_{7-\delta}$ thin film devices," *J. Appl. Phys.*, vol. 91, Apr. 2002, Art. no. 5411.

[11] E. H. Brandt, and M. Indenbom, "Type-II-superconductor strip with current in a perpendicular magnetic field," *Phys. Rev. B*, vol. 48, Nov. 1993, Art. no.12893.

[12] D. Bothner *et al.*, "Magnetic hysteresis effects in superconducting coplanar microwave resonators," *Phys. Rev. B*, vol. 20, Jul. 2012, Art. no. 014517.

[13] P. A. Rosenthal, M. R. Beasley, K. Char, M. S. Colclough, and G. Zaharchuk, "Flux focusing effects in planar thin film grain boundary Josephson junctions," *Appl. Phys. Lett.*, vol. 59, Dec. 1991, Art. no. 3482.

[14] M. Prohammer and J. P. Carbotte, "London penetration depth of d-wave superconductors," *Phys. Rev. B*, vol. 43, Mar. 1991, Art. no. 5370.

[15] S. D. Brorson, R. Buhleier, J. O. White, I. E. Trofimov, H-U. Habermeier, and J. Kuhl, "Kinetic inductance and penetration depth of thin superconducting films measured by THz-pulse spectroscopy," *Phys. Rev. B*, vol. 49, Mar. 1994, Art. no. 6185.

[16] C. J. Fourie, O. Wetzstein, T. Ortlepp, and J. Kunert, "Three-dimensional multi-terminal superconductive integrated circuit inductance extraction," *Supercond. Sci. Technol.*, vol. 24, Nov. 2011, Art. no. 125015.

[17] S. A. Cybart *et al.*, "Large voltage modulation in magnetic field sensors from two-dimensional arrays of Y–Ba–Cu–O nano Josephson junctions," *Appl. Phys. Lett.*, vol. 104, Feb. 2014, Art. no. 062601.

[18] S. A. Cybart, S. M. Anton, S. M. Wu, J. Clarke, and R. C. Dynes, "Very large scale integration of nanopatterned $YBa_2Cu_3O_{7-\delta}$ Josephson Junctions in a two-dimensional array," *Nano Lett.*, vol. 9, Sep. 2009, Art. no. 3581.